Laser-Induced Fluorescence Measurements of Flow Velocity in High-Power Arcjet Thruster Plumes

Daniel A. Erwin* and Gerald C. Pham-Van-Diep†
University of Southern California, Los Angeles, California
and
William D. Deininger‡
Jet Propulsion Laboratory, California Institute of Technology, Pasadena, California

The flow velocity of atomic hydrogen in the plume of an ammonia-propelled arcjet thruster was measured using laser-induced fluorescence (LIF). The velocity was obtained by the Doppler shift of the absorption peak of the Balmer α spectral line. Measurements were made at the nozzle exit, varying the distance from the plume centerline. Results are presented for arcjet operating conditions 13, 20, and 27 kW with a mass flow of 0.31 g/s. The on-axis H flow velocity varies from 14 to 28 km/s over this range of input power. The axial velocity as a function of the distance from the axis is sharply peaked, dropping to almost zero at a radius of less than 5 mm.

Introduction

THIS work presents measurements of axial plume velocity profiles in high-power arcjet thrusters. Arcjets are presently experiencing a revival of interest, as they are expected to play a major role in numerous proposed space missions.[1-6] However, quantitative understanding of arcjet operation is presently quite limited, although recent work on engine simulation has been reported.[7]

Active research on thermal arcjet thrusters began during the late 1950s and proceeded vigorously until the mid-1960s.[8,9] Engines requiring from 1 kW to greater than 200 kW of input power were examined. Engine operation on a variety of propellant gases was investigated and included H_2, He, Li, N_2, NH_3, N_2H_4, Ne, and Ar. Work on arcjet engines stopped during the late 1960s because development work on suitable power sources had ceased. The recent vigorous renewal of development of high-power space power systems, both solar and nuclear, has stimulated interest in using electric propulsion for primary propulsion functions and has led to the renewed development of arcjet engines.

An arcjet engine is one of the simplest electric propulsion devices to build and operate. A schematic of a typical arcjet engine is shown in Fig. 1. The propellant gas is fed into the plenum chamber tangentially, through the chamber wall, and is heated by passing through and around an arc discharge. After the engine is started, a constricted arc in the form of a laminar column extends from the conical tip of the cathode through the constrictor throat, and attaches to the small end of the nozzle. The arc is blown downstream through the constrictor channel by the propellant gas pressure in the plenum chamber. The bulk of the thermal energy is added to the propellant in a thin cylinder along the center line of the device. As a result, the radial distributions of enthalpy and axial velocity are highly peaked at the nozzle exit. Measurements of the radial distribution of mass flux[10] show a minimum on the axis and an increase to a peak at the nozzle edge, with the increase being roughly 10–50% depending on operating power. As noted below, however, these measurements are suspect due to probe intrusion into the flow.

Detailed knowledge of the velocity field produced by an arcjet will provide a greatly improved understanding of engine operation and possibly enable better engine design. Flowfield knowledge, coupled with the mass flux, can yield the inefficiency due to flow nonuniformity. In addition, the frozen-flow loss, i.e., the energy loss due to dissociation, excitation, and ionization of the propellant gas, also requires evaluation to improve understanding of the energy deposition processes at work in an arcjet.

In previous work, impact pressure probes, mass flux probes, and Langmuir probes have been used to measure plume properties in the vicinity of the nozzle opening.[10,11] Such techniques intrude into the flow and consequently cannot be relied upon to provide accurate values. Spectroscopic studies have been performed,[12] but these involve the analysis of emission and precise point-by-point data are difficult to obtain due to difficulties in calibration and data inversion in the highly nonuniform emission produced by arcjets. As will be seen, these difficulties are largely removed by the use of laser-induced fluorescence (LIF).

This report presents results of the first application of LIF to high-power ammonia arject plumes. Radial profiles of the axial velocity of atomic hydrogen are given for engine operation between 12 and 27 kW with a propellant flow rate of 0.3 g/s.

Description of Experiments

Arcjet Facility

The experiments were performed in the JPL Arcjet Testing Facility (ATF). The engine is mounted in a cylindrical, water-cooled stainless steel vacuum tank 1.2 m in diameter and 2.1 m long. The exhaust plume of the arcjet is collected by a 0.16-m diameter diffuser and pumped by a high-capacity vacuum pumping plant based on a 6.3-m^3/s Roots blower. The background tank pressure can be maintained at approximately 0.06 torr during engine operation. The arcjet is mounted on a thrust stand to monitor engine performance during testing. Engine performance and the state of the facility are continuously monitored by a computer-controlled data acquisition system.

Presented as Paper 90-1476 at the AIAA 21st Fluid Dynamics, Plasmadynamics, and Lasers Conference, Seattle, WA, June 18–20, 1990; received Aug. 7, 1990; revision received Jan. 10, 1991; accepted for publication Feb. 11, 1991.
*Assistant Professor, Department of Aerospace Engineering. Member AIAA.
†Research Assistant, Department of Aerospace Engineering. Student Member AIAA.
‡Member of Technical Staff, Electric Propulsion and Plasma Technology Group; currently Senior Scientist, BPD Difesa e Spazio s.r.l., Colleferro, Italy. Member AIAA.

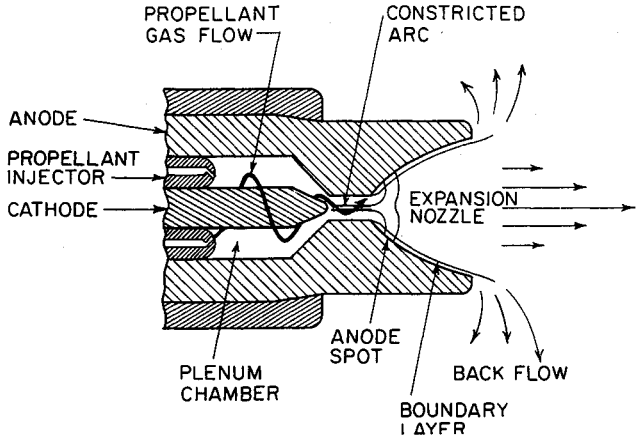

Fig. 1 Arcjet engine operation.

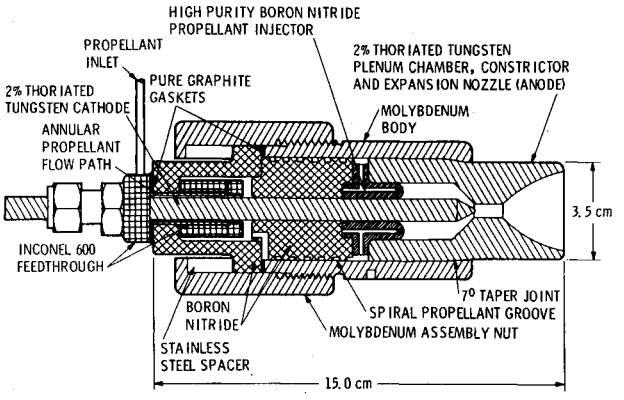

Fig. 3 D-1E arcjet engine.

The ATF is unique in its optical access, with both side-on and end-on windows, as shown in Fig. 2 (The tank is shown with the LIF diagnostic setup installed, which will be discussed below). The end window, possible because of the 90-deg bend in the diffuser, enables direct viewing of the arc while the engine is operating, a capability unmatched elsewhere. Moreover, it allows a laser beam to be admitted parallel to the engine axis, enabling measurement of the plume axial velocity distributions as described later.

The D-1E 30-kW-class ammonia arcjet was used for these tests; it is shown in Fig. 3. This engine is described in detail in Ref. 13. The engine design parameters and essential dimensions are given in Table 1; the important engine features are summarized below. The engine consists of a single-piece plenum chamber/constrictor/expansion nozzle machined from 2% thoriated tungsten. The constrictor is nominally 1.08 cm long by 0.5 cm in diameter with a nominally 50-deg half-angle cone at its inlet. (The constrictor inlet was recently remachined to a double taper. This is not shown in Fig. 3.)

Table 1 Design parameters and essential dimensions of arcjet engine used

Parameter	D-1E Engine
Constrictor length, cm	1.08
Constrictor diameter, cm	0.50
Nozzle exit diameter, cm	2.93
Exit area ratio[a]	33
Nozzle type	Bell
Outer nozzle surface material	W
Plenum chamber diameter, cm	2.03
Plenum half-angle taper at constrictor end, deg	49.5
Cathode diameter, cm	0.95
Cathode tip included angle, deg	60
Cathode tip radius, cm	0.15
Electrode gap,[b] cm	0.21
Propellant injection angle from axis, deg	60
Nominal engine diameter, cm	5.08
Nominal engine length, cm	15.0

[a]Ratio of nozzle exit area to constrictor area.
[b]Axial gap between the cathode cone and the corner of the constrictor entrance.

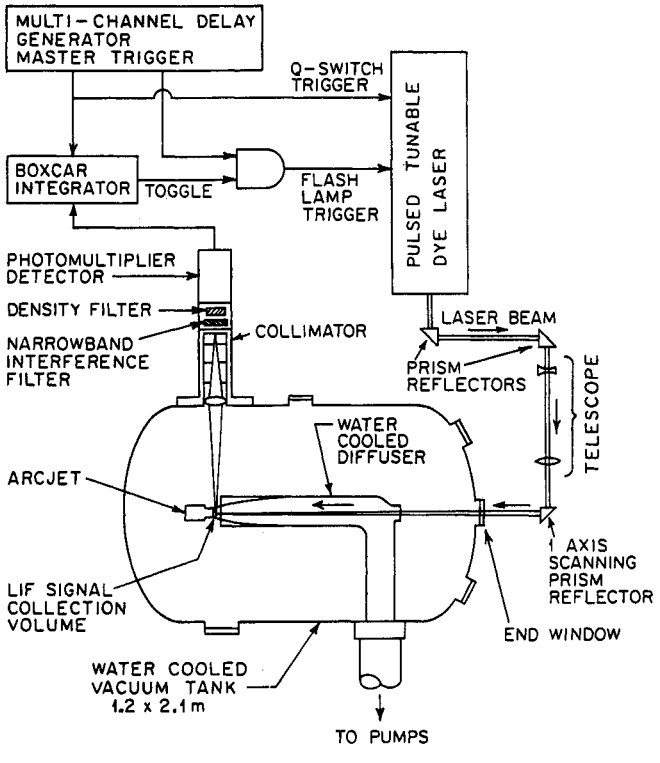

Fig. 2 Arcjet vacuum facility, with the LIF setup installed.

The nozzle is bell-shaped with an area ratio of 33. A boron nitride insulator between the cathode and anode also serves as the injector. The propellant is injected, with a downstream inclination 60 deg from the axis, at the back of the plenum chamber through four 0.15-cm diameter injection holes. The cathode, made from 2% thoriated tungsten, has a 60-deg included-angle cone-shaped tip out to its 0.95-cm diameter.

The performance of the arcjet is given in Table 2. Data are given for the three power levels at which velocities were measured. The specific impulse I_{sp} is given in km/s to facilitate comparison with the measured velocities.

LIF Measurement Technique

Arcjet plumes present excellent conditions for measuring particle velocities using Doppler shifts. As will be seen, velocities may be measured with a precision of about 1 km/s. In our case, since ammonia is the propellant, excited states of atomic hdyrogen are present, which may be observed in emission or probed using LIF. The density is thought to be sufficiently low that atomic transition lines are not significantly broadened by collisions with particles other than electrons. The plume is believed to be field-free, so that there is no DC Stark splitting. The transitions are thus affected only by Doppler shift and by Doppler and Stark (electron collisional) broadening.

This work employed LIF to measure the radial profiles of the arcjet plume axial velocity at the nozzle exit. Each molecular species in the plume has a different velocity; this work deals specifically with the velocity of atomic hydrogen. The

Table 2 Summary of operating conditions for presented results

Power, kW	Current, A	Voltage, V	Mass flow, g/s	Thrust, g	I_{sp}, km/s
27.1	249	109	0.315	225	7.00
20.2	181	111	0.315	200	6.22
13.1	124	106	0.315	143	4.45

velocity was obtained by measuring the Doppler shift of the broadened atomic hydrogen Balmer α spectral line in absorption.

The Balmer α line, of wavelength $\lambda_0 = 6563$ Å, joins the $n = 2$ and $n = 3$ energy levels of the H-atom. The ammonia arcjet plume appears red to the eye, largely due to this line. In the present LIF technique, absorption of light from a pulsed tunable dye laser (pulse length ~10 ns) increases the population density N_3 of atoms in the $n = 3$ level. This increase causes a momentary increase in the Balmer α emission, which is the LIF signal. The excess density decays to its original value through radiation and through collisional excitation/de-excitation to other levels. This is expressed by the rate equation

$$\frac{dN_3}{dt} = (N_2B_{23} - N_3B_{32})I\frac{\lambda^2}{c^2}g(\lambda) - (N_3 - N_3^0)\left(\sum_i S_{3i} + A_{32} + A_{31}\right) \quad (1)$$

The first pair of parentheses on the right contains the terms that are due to laser action. These are the absorption (pumping) and stimulated emission rates, $2 \rightarrow 3$ and $3 \rightarrow 2$, respectively. B_{23} and B_{32} are the Einstein coefficients of absorption and stimulated emission,[14] I is the laser intensity (assumed monochromatic with wavelength λ), c is the speed of light, and $g(\lambda)$ is the lineshape of the $2 \rightarrow 3$ transition, area-normalized to unity ($\int g(\lambda)d\lambda = 1$). The terms following the pumping term give the rate of decay of the difference between N_3 and its steady-state (pre- and postlaser irradiation) value N_3^0. S_{3i} gives the rate for collisional transition to a state i. $A_{32} = 4.4 \times 10^7\ s^{-1}$ is the Einstein spontaneous emission coefficient for $3 \rightarrow 2$ (Balmer α) radiation, and A_{31} is the coefficient for emission to the ground state.

In this work, only the peak wavelength of the transition is of interest, rather than the magnitude of the LIF signal. The values of the collisional terms S_{3i} therefore do not affect these results, nor does reabsorption of $3 \rightarrow 1$ emission. Moreover, the light collection system need not be calibrated except to assure linearity.

The lineshape $g(\lambda)$ contains the effects of collisions (primarily with electrons) and of Doppler shifts due to random atomic motion (thermal or turbulent) in the width and shape of the profile; the effect of bulk atomic velocity is a shift of the peak of the line from its zero-velocity value λ_0. In cases where either collisional (Stark) broadening or Doppler broadening is clearly dominant over the other, the linewidth can provide a measure of either electron density or translational temperature. In the present case, both broadening mechanisms contribute. The results given here, however, are affected additionally by power broadening,[14] so the observed linewidth is considerably greater than that which would be observed in emission. For this reason, we do not present analysis based on the linewidth but consider only the peak positions.

The random motion and the flow velocity enter through the Doppler shift of the absorption profile, so only the velocity components *in the direction of the laser beam* (parallel to the engine axis in this work) enter in. In this experiment, the atomic velocity perpendicular to the laser beam does not play a role, as the wavelength dependence of the LIF emission is not monitored.

The laser wavelength is scanned across the Balmer α transition to obtain the LIF signal as a function of wavelength. The atomic hydrogen flow velocity is obtained from the shift of the peak of the LIF signal from λ_0 by

$$v = \frac{\Delta\lambda}{\lambda_0}c \quad (2)$$

where $\Delta\lambda$ is the shift of the profile peak with respect to λ_0. Thus a peak shift of 0.1 Å corresponds to a flow velocity of 4.6 km/s for Balmer α pumping. (The flow is toward the laser source, so the shift is in the direction of increasing wavelength.) Arcjet plume velocities are very high, of order 20 km/s, corresponding to a transition lineshift of order 0.4 Å.

LIF has been performed using the Balmer lines in a variety of applications.[15-20] Electron densities have been measured[21] in hydrogen thyratrons using weakly pumped LIF to obtain the Stark linewidth[22,23] of Balmer β (λ = 4861 Å), whose dependence on electron density is well known[22]; there, the shift of the line was not measured, as the plasma was confined and no bulk high-speed flow was possible. The present work employed the Balmer α line, rather than the Balmer β line, to maximize the experimental sensitivity, shown by Eq. (2) to be proportional to the wavelength.

To measure the axial flow velocity as a function of radius (distance from the plume axis), the variation of the LIF signal with wavelength was obtained as described above, for various radial positions of the laser beam. During each scan of the laser wavelength, the fluorescence from a small volume along the beam was collected and recorded. (See Fig. 2.) Since the plume conditions remain generally constant on a time scale of hours, the requirements on the speed of the scan are not stringent.

The LIF signal at each radial position and laser wavelength was averaged over 100 samples to suppress noise due to laser power fluctuation. The signal consisted of a constant offset due to the background plume emission and to directly scattered laser light as well as the wavelength-dependent LIF signal; since the pump and signal transitions are the same, differentiation between LIF and scattered laser photons is impossible. The resulting intensity-vs-wavelength profile, with the offset subtracted, is the absorption lineshape if the laser pumping is sufficiently weak. This condition was checked by repeating a scan with larger laser powers; an increase by a factor of 4 in the laser pulse energy led to a broadening of about 10%. The measured profiles thus contain some power broadening. Laser pulse energies used were generally about 0.1 mJ.

The position of the profile peak was obtained by fitting the data points with an assumed profile, Gaussian, Lorentzian, or polynomial. (This will be discussed in detail below.) The flow velocity corresponding to a peak position is given by Eq. (2). Note that the experiment provides no absolute reference of wavelength, so that zero velocity must be inferred by the peak position at the edge of the plume.

The flow velocity is obtained at a variety of radial positions by moving the laser beam horizontally as described. This could be done with a precision of an estimated 0.5 mm. Thus the velocity-vs-radius data points are characterized by a random horizontal error of 0.5 mm. In addition, the resulting profile must be considered to be convolved with an instrument function of full width approximately 0.6 mm due to the laser beam size.

Experimental Setup

The velocity component of primary interest is the streamwise (axial) one, requiring the laser beam to be parallel to the axis of the arcjet, as shown in Fig. 2. The laser beam enters through the port at the downstream end of the tank; its displacement from the axis is controlled by the orientation of the scanning prism, which was mounted on a motor-driven rotation stage so that the beam could be translated horizontally across the plume.

The laser used was a Quanta-Ray PDL-1 side-pumped, grating-tuned, pulsed dye laser, whose output linewidth was about 0.04 Å. The dye laser was pumped by a frequency-doubled Quanta-Ray DCR-1 flashlamp-pumped Nd:YAG laser. Output pulse energies of order 100 mJ in 10 ns at 6563 Å could be obtained, but as already discussed, much lower energies were appropriate for this experiment. The pulse-to-pulse energy stability was poor, the fluctuations ranging as high as 30%.

The laser beam was apertured to a diameter of 2 mm at the exit of the dye laser; a two-lens telescope was used to give a spot size of about 0.6 mm at the engine nozzle. Light from the nozzle area was collected using a positive lens at the inlet of the collimator. The resulting cone of light was apertured by the clearance between the nozzle exit and the diffuser, which was about 6 mm. Thus LIF signal was obtained from a cylinder approximately 0.6 mm in diameter and 6 mm in length. Non-Balmer α light was rejected by a narrow-band interference filter (Melles Griot, $\lambda = 6560$ Å, $\Delta\lambda = 100$ Å). In order to avoid detector saturation, two or so orders of neutral density filters were used.

Light was detected by an EMI 9789-QB photomultiplier, thermoelectrically cooled to 5°C, supplying current to a boxcar averager (Stanford Research) with a 50-ohm terminating resistor in place. The boxcar operated in the toggle (background subtract) mode, triggering at twice the laser pulse frequency of 10 Hz. Timing for the experiment was based on the lamp-firing pulse of the laser. The first data were taken with the laser Q-switch internally triggered, which gave a large pulse jitter and drift; this required the boxcar gate to be wide (200 ns) and centered on the apparent mean pulse time. Later, external triggering of the Nd:YAG laser Q-switch suppressed the pulse jitter to less than 2 ns, allowing a lower gate width to be used. A gate width of 50–100 ns was found optimal.

Results and Discussion

We present results for a number of different engine operating conditions. These are summarized in Table 2. Results are presented in Figs. 4–7 for operating conditions of 13, 20, and 27 kW. Both raw data (typical intensity-vs-wavelength profiles) and the corresponding velocity profiles are presented. Profiles are given for several values of the distance r from the plume centerline. The data points are shown along with least-squares best-fit Gaussian and Lorentzian profiles. Random vertical errors result from laser pulse energy variation, which causes fluctuations in both the LIF signal and the directly scattered laser light. In addition, a slight error arises from timing jitter. The signal level is high enough that shot noise and dark-current noise are not significant compared to the other sources of error. The random error in the wavelength is assumed negligible, but the absolute wavelength must be determined as discussed previously by the position of the profile at the plume edge. The linewidth of the laser was about 0.04 Å, so that the measured profiles are convolved with a profile of that width; the effect of this on the peak positions, and hence on the velocity results, is insignificant since the profiles are close to symmetric. It should also be noted that the measured profiles are axial averages over the 6-mm nozzle-diffuser spacing.

The profiles measured here have full widths at half maximum (FWHMs) ranging from 1.1 to 1.7 Å, increasing with power level. Observation of the Balmer α line in emission, under similar arcjet plume conditions (power 20 kW, mass flow 0.25 g/s),[12] gave linewidths of about 0.5 Å. In the majority of cases, the χ^2 measure of least-squares best fit[24] slightly favored the Gaussian over the Lorentzian shape, but the differences are not significant.

The velocity results presented assume a Gaussian fit to the LIF profiles; this choice is rather arbitrary, as Figs. 4–6 show. The differences between these results and those obtained with the other fitting methods are small, falling well within the error bars representing the uncertainties of the Gaussian peak positions (see below).

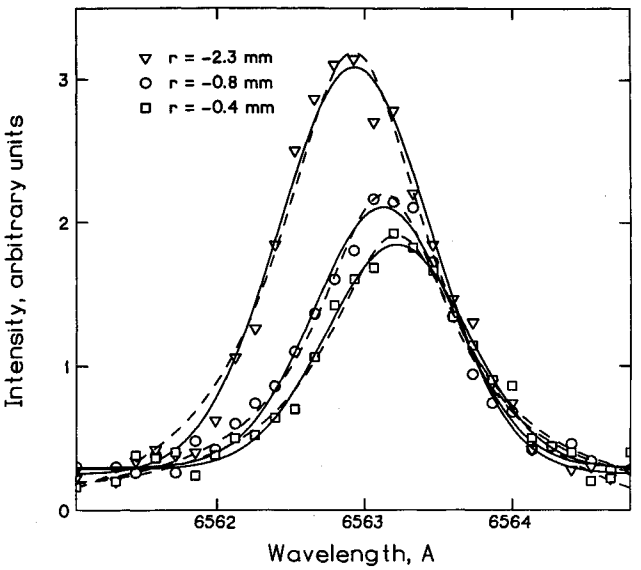

Fig. 4 Raw LIF data taken during operation at 13 kW. *Solid curve*, best-fit Gaussian; *dashed curve*, best-fit Lorentzian.

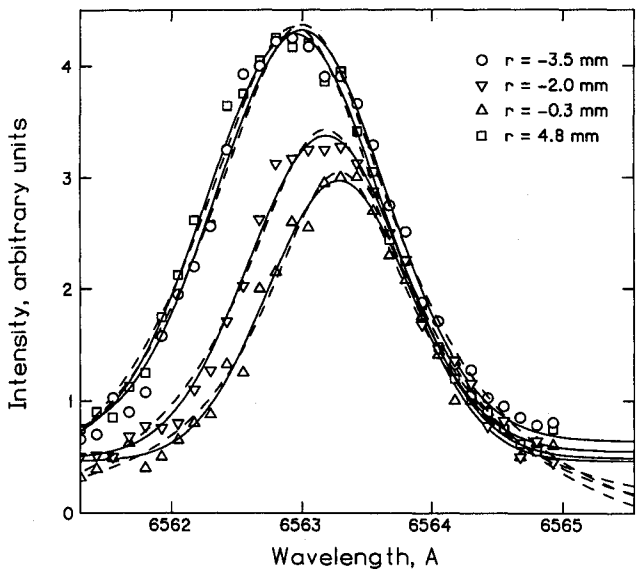

Fig. 5 Raw LIF data taken during operation at 20 kW. *Solid curve*, best-fit Gaussian; *dashed curve*, best-fit Lorentzian.

The engine configuration was constant during the acquisition of these data; in fact, the data were taken continuously, with the only variation being the power level. The highest power data were taken first to minimize the effect of electrode erosion, which would cause a drift in the results. Examination of the engine following the runs did not show significant erosion. Because of this, these data accurately characterize the variation of plume velocity and shape with operating power.

In Fig. 7, the horizontal error bars represent the reproducibility error of the beam turning prism rotator, estimated to be 0.5 mm in the nozzle exit plane. The vertical error bars correspond to the uncertainty in the peak positions of the Gaussian fits to the LIF profiles. This uncertainty was obtained from the covariance matrix[24] of the least-squares fit, assuming normally distributed scatter in the raw data.

Figure 7 shows a rapid increase in peak velocity with power. In fact, for this mass flow rate, the relation 1 km/s per kilowatt describes the data fairly well. Moreover, the high-speed core

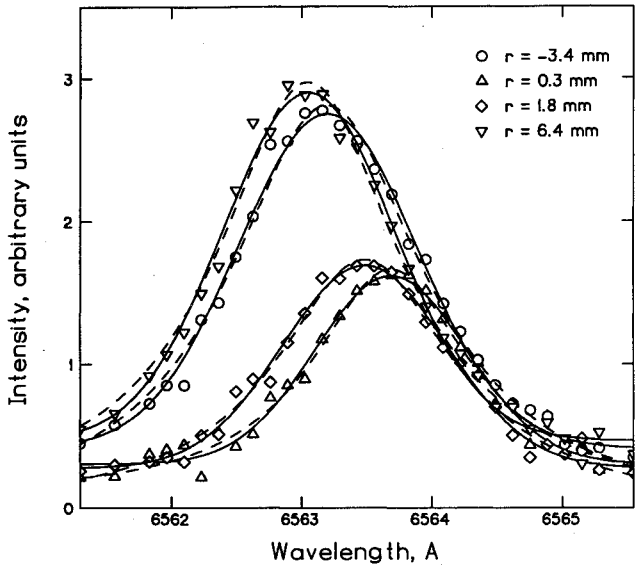

Fig. 6 Raw LIF data taken during operation at 27 kW. *Solid curve*, best-fit Gaussian; *dashed curve*, best-fit Lorentzian.

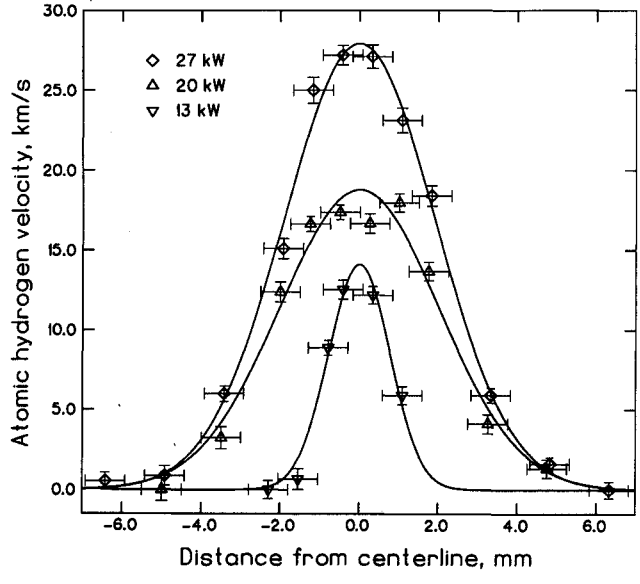

Fig. 7 Velocity vs distance from plume centerline, for operation at 13, 20, and 27 kW.

of the plume broadens with increasing power, though the variation is not linear and appears to flatten at high power. This is consistent with the measured thrust (Table 2) which shows a much greater increase between 13 and 20 kW than between 20 and 27 kW.

In all cases, the peak velocities are considerably higher than the average velocities obtained from thrust measurements (the average velocities are given as I_{sp} in Table 2). It must be re-emphasized that the measured velocities are of atomic hydrogen only. There is an unknown, but probably significant, difference between the H velocity and those of heavier species. Moreover, the high-speed core of the plume carries an unknown fraction of the total mass flux. A logical extension of the present work would measure the velocity of atomic nitrogen, retaining ammonia as the propellant; another would be the measurement of the flow velocity of a single-species propellant such as helium. In any case, the development of a nonintrusive technique to measure mass flux per unit area across the nozzle exit (species-specific in the case of a molecular propellant) is needed, along with the present technique, to fully address this problem.

Conclusions

The ability of LIF to produce good-quality (± 1 km/s), nonintrusive plume velocity measurements in high-power arcjet plumes has been demonstrated. Axial atomic hydrogen velocities obtained using LIF exhibit much lower error bars than earlier measurements, as well as much better spatial resolution.

A self-consistent study (identical engine configuration throughout) of the variation of plume shape and velocity with operating power shows a close-to-linear increase in centerline velocity with power. However, the thrust does not increase linearly. The data presented here indicate that, for this engine at least, specific impulse does increase with power, but that this benefit is partially offset by increasing flow nonuniformity at high power. A full treatment of this problem will require further work as outlined at the end of the previous section.

Acknowledgments

This work was supported by the Caltech President's Fund and the SDIO. The authors thank R. Toomath and W. Thogmartin for expert electronic and facilities support, and Keith Goodfellow for much unpaid assistance, also expertise.

References

[1]Mudt, J. F., "Multimission NEP System for Outer Planet Exploration Missions," 15th IEPC, AIAA Paper 81-0698, April 1981.

[2]Rutkowski, E. F., and Kaplan, M. H., "A Nuclear Electric Transfer for Nuclear Waste Disposal," 15th IEPC, AIAA Paper 81-0706, April 1981.

[3]Garrison, P. W., "Advanced Propulsion for Future Planetary Spacecraft," *Journal of Spacecraft and Rockets*, Vol. 19, 1982, p. 534.

[4]Phillips, W. M., "Nuclear Electric Power System for Solar System Exploration," *Journal of Spacecraft and Rockets*, Vol. 17, 1980, p. 348.

[5]Vondra, R. J., Nock, K., and Jones, R. M. "A Review of Electric Propulsion Systems and Mission Applications," Proceedings of the 17th IEPC, IEPC Paper 84-82, Tokyo, July 1984.

[6]Deininger, W. D., and Vondra, R. J., "Development of an Arcjet Nuclear Electric Propulsion System for a 1993 Flight Demonstration," 22nd Joint Propulsion Conference, AIAA Paper 85-2031, June 1986.

[7]Butler, G. W., Kashiwa, B. A., and King, D. Q. "Numerical Modeling of Arcjet Performance," 21st Fluid Dynamics, Plasma Dynamics and Lasers Conference, AIAA Paper 90-1474, June 1990.

[8]Wallner, L. E., and Czika, J., Jr., "Arcjet Thruster for Space Propulsion," NASA TN D-2868, June 1965.

[9]Pivirotto, T. J., and King, D. Q. "Thermal Arcjet Technology for Space Propulsion," JANNAF Propulsion Meeting, San Diego, CA, 1985.

[10]VanCamp, W. M., Esker, D. W., Checkley, R. J., Duke, W. G., Kroutil, J. C., Merrifield, S. E., and Williamson, R. A., "Study of Arcjet Propulsion Devices," Final Report, McDonnell Rept. E 368, NASA CR-54691, March 1966.

[11]Limbaugh, C. C. "Determination of the Excited State Density Distribution with a Nonequilibrium Freely Expanding Argon Arcjet Plume," Final Report, AEDC-TR-66-139, March 1977.

[12]Pivirotto, T. J., and Deininger, W. D. "Velocity Measurements in the Plume of an Arcjet Engine," 19th IEPC, AIAA Paper 87-1063, May 1987.

[13]Deininger, W. D., Chopra, A., King, D. Q., and Pivirotto, T. J., "Thermal Design Improvements for 30 kW Arcjet Engines," 20th IEPC, IEPC-88-073, 1988.

[14]Demtröder, W., *Laser Spectroscopy: Basic Concepts and Instrumentation*. Springer-Verlag, Berlin, 1988.

[15]Erwin, D. A., and Gundersen, M. A., "Laser-Induced Fluorescence Diagnostics in High-Current Plasmas," 38th Gaseous Electronics Conference, Monterey, CA, 1985.

[16]Erwin, D. A., and Gundersen, M. A., "Measurement of Excited-State Densities During High-Current Operation of a Hydrogen Thyratron Using Laser-Induced Fluorescence," *Applied Physics Letters*, Vol. 48, 1986, p. 1773.

[17]Burgess, D. D., Kolbe, G., and Ward, J. M., "Direct Laser-Based Measurements of the Collisional Depopulation Rate of the

$n=2$ Level of Hydrogen in a Plasma," *Journal of Physics B: Atomic and Molecular Physics*, Vol. B11, 1978, p. 2765.

[18]Burgess, D. D., Myerscough, V. P., Skinner, C. H., and Ward, J. M., "A Comparison Between Theory and Laser Spectroscopic Measurements for a Hydrogen Plasma Under High-Intensity Resonant Balmer Irradiation," *Journal of Physics B: Atomic and Molecular Physics*, Vol. B13, 1980, p. 1675.

[19]Razdobarin, G. T., Semenov, V. V., Sokolova, L. V., Folomkin, I. P., Burakov, V. S., Misakov, P. Ya, Naumenkov, P. A., and Nechaev, S. V., "An Absolute Measurement of the Neutral Density Profile in the Tokamak Plasma by Resonance Fluorescence on the H_α Line," *Nuclear Fusion*, Vol. 19, 1979, p. 1439.

[20]Gohil, P., Kolbe, G., Forrest, M. J., Burgess, D. D., and Hu, B. Z., "A Measurement of the Neutral Hydrogen Density Determined from Balmer Alpha Fluorescence Scattering in the HBTX1A Reverse Field Pinch," *Journal of Physics D: Applied Physics*, Vol. D16, 1983, p. 333.

[21]Braun, C. G., Erwin, D. A., and Gundersen, M. A., "Fundamental Processes Affecting Recovery in Hydrogen Thyratrons," *Applied Physics Letters*, Vol. 50, 1987, p. 1325.

[22]Vidal, C. R., Cooper, J., and Smith, E. W., "Hydrogen Stark-Broadening Tables," *Astrophysical Journal Supplement Series*, Vol. 25, 1973, pp. 37–136.

[23]Burgess, D. D., Kolbe, G., and Playford, C. St.Q., "Long Path Absorption Measurements of the Pressure-Broadened Balmer-Alpha Profile," in *Spectral Line Shapes*, edited by B. Wende, Walter de Gruyter, Berlin, 1981.

[24]Press, W. H., Flannery, B. P., Teukolsky, S. A., and Vetterling, W. T., *Numerical Recipes: The Art of Scientific Computing*. Cambridge Univ. Press, Cambridge, England, UK, 1986.